ELSEVIER

International Journal of Mass Spectrometry 205 (2001) 253–270

International Journal of Mass Spectrometry

Investigations of low energy electron attachment to ground state group 6B hexafluorides (SF_6, SeF_6, and TeF_6) using an electron-swarm mass spectrometric technique

G.K. Jarvis[a], R.A. Kennedy[b], C.A. Mayhew[a,*]

[a]*School of Physics and Astronomy*, [b]*School of Chemistry*
University of Birmingham, Edgbaston, Birmingham B15 2TT, United Kingdom

Received 28 January 2000; accepted 30 March 2000

Abstract

Studies of low energy electron attachment to SF_6, SeF_6, and TeF_6 have been carried out in an atmospheric pressure nitrogen buffer gas (number density N) at 300 K. The experiments are conducted under nonthermal electron-swarm conditions, using an instrument that combines an atmospheric pressure drift tube, with a quadrupole mass spectrometer. Details of the design, construction and operation of the drift tube and the associated fast electron gate are presented. Electron drift times can be measured, and mean electron drift velocities in N_2 as a function of the density reduced electric field strength E/N are reported. Density normalised electron attachment coefficients, α, and electron attachment rate constants, k_a, together with product anion branching ratios (for SeF_6 and TeF_6) are determined as a function of E/N. The studies presented here cover the range $E/N = (0.4–17) \times 10^{-18}$ V cm^2, corresponding to mean electron energies of 0.04–0.6 eV. For all three molecules, k_a decreases as E/N increases. SF_6 attaches electrons much more rapidly than either SeF_6 or TeF_6. The ratios $k_a(SF_6)$:$k_a(SeF_6)$:$k_a(TeF_6) \approx 3000$:10:1 are found not to vary with E/N. The estimated thermal (300 K) electron attachment rate constants are $k_{th}(SF_6) \approx (2.5 \pm 0.3) \times 10^{-7}$ cm^3 s^{-1}, $k_{th}(SeF_6) \approx (8.0 \pm 1.2) \times 10^{-10}$ cm^3 s^{-1}, and $k_{th}(TeF_6) \approx (8.2 \pm 1.1) \times 10^{-11}$ cm^3 s^{-1}. For all three molecules, attachment is dominated by the capture of near-zero-energy electrons. In each case the dominant anion product is XF_6^- (X = S, Se, Te), accompanied by XF_5^-. No other anion products directly arising from electron attachment to XF_6 are observed. Extrapolation of the relative product anion intensities to zero attaching gas concentration yields the following branching ratios for attachment under swarm conditions: SeF_6–SeF_5^- (20%), SeF_6^- (80%); and TeF_6–TeF_5^- (3%), TeF_6^- (97%). These ratios are found to be independent of E/N. The observation of SeF_6^- and TeF_6^- as the dominant anions from SeF_6 and TeF_6 is ascribed to stabilisation of the initial anion formed by electron capture through collisions with the nitrogen buffer gas. For SF_6, the observed proportion of SF_5^- decreases from 8% to 1% over the E/N range of this study, whereas an increase in the SF_5^- branching ratio with E/N is anticipated from previous low-pressure, electron beam investigations. (Int J Mass Spectrom 205 (2001) 253–270) © 2001 Elsevier Science B.V.

Keywords: Electron attachment, Rate constants; Electron swarms; SF_6, SeF_6, TeF_6

1. Introduction

Free electron attachment to neutral molecules leads to the formation of anions:

$$e^- + MY_n \rightarrow (MY_n^-)^*. \quad (1)$$

* Corresponding author. E-mail: c.mayhew@bham.ac.uk

Dedicated to Professor Alex Stamatovic in honour of his 60th birthday and in recognition of his major contributions to the study of low energy electron-molecule interactions.

1387-3806/01/$20.00 © 2001 Elsevier Science B.V. All rights reserved
PII S1387-3806(00)00277-3

The excited parent anion may be collisionally stabilised:

$$(MY_n^-)^* \xrightarrow{\text{buffer gas}} MY_n^- \quad (2)$$

dissociate (as a result of collisions or spontaneously):

$$(MY_n^-)^* \xrightarrow{\text{buffer gas}} \begin{cases} MY_{n-1}^- + Y \\ MY_{n-1} + Y^- \end{cases} \quad (3a)$$

$$(MY_n^-)^* \rightarrow \begin{cases} MY_{n-1}^- + Y \\ MY_{n-1} + Y^- \end{cases} \quad (3b)$$

or it may autodetach:

$$(MY_n^-)^* \rightarrow e^- + MY_n. \quad (4)$$

This production of anions is an important process in plasmas, for it influences the plasma's free-electron number density. Furthermore, the presence of anions can reduce the plasma's cation number density directly through anion–cation neutralisation and indirectly by anion–neutral reactions. This is considered to be a problem in many types of plasma processing because of the corresponding reduction in the positive ion flux to the substrate [1].

Many sequential and parallel chemical reactions involving charged species occur in a plasma. Therefore a large database of various cross sections and rate constants of electron–molecule, electron–ion recombination, anion–cation neutralisation, and ion–molecule processes is required to model a plasma's chemical and physical environment. Modeling could be used, for example, to propose ways in which a plasma's electron and ion number densities might be optimised in order to enhance critical plasma parameters.

It is very difficult, if not impossible, to obtain much needed data directly from a plasma, given that so many sequential and parallel reactions occur. Therefore, experimental techniques have been developed which permit the measurement of data isolated from the plasma's environment, usually in which only one process is occurring, and in which only one or two species are involved. The objective of our studies is to use an electron-swarm technique to extend the available experimental database on attachment of low energy electrons to molecules.

In this article, we describe a nonthermal electron-swarm technique to investigate electron attachment processes. Such a technique does not directly measure electron attachment cross sections, $\sigma(\epsilon)$, as a function of electron energy, ϵ, but rather "total attachment cross sections" for a given distribution of electron energies, which may in part be characterised by a mean electron energy, $\bar{\epsilon}$. If the electron energy distribution is well known, deconvolution of the data can in theory lead to a determination of $\sigma(\epsilon)$. However, any deconvolution method is subject to many uncertainties. It may therefore be safer, and perhaps more than sufficient when modeling a plasma, to use only "total attachment cross sections" and their variations with reduced electric field strength, E/N (where E is the electric field strength and N is the total molecular number density) [2]. Electron-swarm techniques are ideal for such measurements. Density normalised attachment coefficients (the total attachment cross sections), $\alpha(E/N)$, are routinely measured by such a technique, and from these the more useful electron attachment rate constants, $k_a(E/N)$, can be determined [3,4].

Recently, our electron-swarm mass spectrometric instrument [5] has been modified, improving in particular its operation in the region of mean electron energies close to the thermal value ($\bar{\epsilon} = \frac{3}{2}k_BT$). Other improvements include greater sensitivity, the ability to measure mean electron drift velocities (for $E/N < 2 \times 10^{-18}$ V cm^2) and access to a larger range of E/N. These improvements are described in some detail in this article. The instrument's performance is illustrated here by presenting an investigation of electron attachment to three hexafluorides, namely SF_6, SeF_6, and TeF_6 in their ground electronic states at 300 K. Our main aim is to compare and contrast the electron attachment results from these three structurally similar compounds. A unique aspect of our instrument is that the anion products resulting from electron attachment under swarm conditions are recorded, and the anion product branching ratios for electron attachment to SeF_6 and TeF_6 are presented in this article.

There have been numerous studies of electron attachment to SF_6 [6–14], mainly because of its use as a high voltage insulator. SF_6 has a large rate constant

for low energy electron attachment. For example, the thermal electron attachment rate constant at 300 K, has been determined to be $(3.1 \pm 0.5) \times 10^{-7}$ cm^3 s^{-1}, which is close to the theoretical maximum [6]. Thus, it readily mops up low energy free electrons, and thereby inhibits electrical breakdown. Further motivation for the study of electron attachment to SF_6 comes from its use in plasma-etching applications in industry [15–21]. A thorough understanding of the electron attaching properties of SF_6 and its reactions with anions (and cations) is important for modeling and characterising such plasmas [22].

In comparison to SF_6, fewer studies dealing with the electron attachment properties of SeF_6 and TeF_6 appear in the literature. There have been a number of low-pressure electron beam studies [23–27], but to our knowledge, only one electron-swarm study [28]. This early swarm study only measured the thermal electron attachment rate constants by use of a drift–dwell–drift technique in low pressures of the pure electron attaching gas. Thus, electron-swarm measurements for SeF_6 and TeF_6 covering a range of mean electron energies (0.04–0.6 eV) are presented here.

2. Experimental

2.1. Electron-swarm technique

The electron-swarm technique for the study of electron attachment processes has been described in detail in the literature [3,4]. In brief, a pulsed swarm of electrons, produced at one end of a drift tube, is drawn through an inert buffer gas of number density N, under the influence of a uniform electric field of magnitude E, to a collector. The electrons within the pulse quickly reach an equilibrium energy distribution. This distribution of electron energies arises from competition between the energy gained from the accelerating electric field and the energy lost in collisions with the buffer gas. The electron energy distribution is thus dependent on E/N, the type of buffer gas used (commonly He, N_2, or Ar), and temperature. Very small admixtures (usually less than one part per million) of an attaching gas, M, in the buffer gas result in the removal of electrons from the pulse, and hence a reduction in the electron current. These small concentrations of electron attaching gas are assumed not to alter the electron energy distribution.

By monitoring the amplitude of the electron pulse as a function of attaching gas concentration $[M]$, the density normalised electron attachment coefficient, $\alpha(E/N)$, can be extracted from the exponential attenuation equation:

$$\frac{A}{A_0} = \exp(-\alpha l[M]) \tag{5}$$

where A and A_0 are, respectively, the pulse amplitudes with and without attaching gas in the drift tube, which is of length l.

From the measured $\alpha(E/N)$, the electron attachment rate constant, $k_a(E/N)$, can be calculated using the mean electron drift velocity, $w(E/N)$:

$$k_a = w\alpha. \tag{6}$$

Given adequate time resolution, $w(E/N)$ can be obtained from the time taken for an electron pulse to pass through the drift tube. Alternatively, extensive tabulations for $w(E/N)$ for various buffer gases are available in the literature [10].

Anions are formed throughout the drift tube, with the number generated decreasing as the electron pulse propagates through the tube. The huge mass difference between an electron and an anion ensures that anion mean drift velocities are more than 10^3 times less than electron mean drift velocities. The anion current will thus be of lower amplitude and temporally distinct from the pulse of current due to the electrons; the anions appear as a long, low tail after the electron pulse. Hence, the contribution of the anions to the recorded signal can be rejected, and so ignored in the determination of α.

2.2. Birmingham electron-swarm apparatus: general details

The basic principles of the apparatus used in this study have been presented previously [5]. However, as was mentioned in sec. 1, the apparatus has recently

been modified to improve its performance, and these modifications will now be described.

The apparatus discussed in [5] was an adapted ion-mobility mass spectrometer, designed to operate at $E/N > 2 \times 10^{-18}$ V cm^2. In electron-swarm mode, this corresponds to mean electron energies in a nitrogen buffer gas of $\bar{\epsilon} > 0.09$ eV. At lower E/N, electron gating, which is an integral part of the electron-swarm technique, proved problematic. Also pronounced charging phenomena, whereby electron pulses took many minutes to come to a constant amplitude, were observed at low E/N.

Many molecules, important in plasmas and discharges, strongly attach low energy electrons, and therefore it is important to be able to reliably operate the apparatus in the low E/N regime ($<2 \times 10^{-18}$ V cm^2). In particular, we wish to operate our drift tube under conditions where the electrons are, to a good approximation, in thermal equilibrium with the surrounding buffer gas. At 300 K, a thermal electron swarm will have a mean electron energy of 0.038 eV. To attain such a mean electron energy, with nitrogen as the buffer gas, requires $E/N < 3 \times 10^{-19}$ V cm^2 [10].

In the original instrument, the drift tube consisted of a glass cylinder with ring electrodes clamped to its outer surface. Potentials were applied to the rings to give a uniform E field along the axis of the drift tube. The observed charging phenomena were thought to be a direct consequence of the glass cylinder. Charging up of the glass might have caused distortions in the E field, which are undesirable if we are to have a well-characterised electron swarm. In the new drift tube, the glass cylinder, which is used to constrain the gas flows, has been moved outwards and the ring electrodes brought inside to minimise charging effects. In addition a new electron gate has been designed and produced. This gate operates over a wide range of E/N, and has several other beneficial characteristics. Details of the new drift tube and electron gate are described in sec. 2.3.

2.3. Drift tube

This represents the first major change to the original instrument. Fig. 1 shows a schematic diagram of the new drift tube. A 70 μm hole in the centre of our collector, the Faraday plate (see Fig. 1), leads to the unmodified part of the instrument—the differentially pumped chamber and the quadrupole mass spectrometer. (A description of these is given in [5].)

As mentioned previously, the new design uses metal ring electrodes inside a cylindrical glass envelope. Importantly, we have not observed any charging phenomena with the new drift tube. A negative high voltage is applied to the electron gate and its holder. Fifteen metal ring electrodes, each of internal diameter 5 cm and thickness 5 mm, follow the gate. Each electrode ring is made of aluminium, and is molybdenum coated to reduce charging effects [29]. They are physically separated from each other by 1 mm ceramic spacers, but are electrically connected in series via a chain of 10 MΩ resistors. The ceramic spacers are placed nearer to the outer part of the electrodes, to minimise the possibility of charging effects. The entire drift tube is of length 9.8 cm, measured from the electron gate to the Faraday plate. It is supported by four 1.6 mm threaded rods, electrically isolated from the ring electrodes by ceramic sleeves. The rods are screwed into the end plate, which is in contact with the rest of the chamber, and hence is maintained at ground potential. The Faraday plate is electrically isolated, but was held at ground potential for all the experiments presented here.

With the above-mentioned design, the electric field established within the drift tube is expected to be highly uniform between the electron gate and the Faraday plate. Modeling of the electric potential distribution using the programme SIMION [30] confirms this expectation.

Nitrogen, or any other gas that does not attach electrons and provides a known electron energy distribution for a given E/N, can be used as the buffer gas. The pressure in the drift tube is maintained at slightly above 1 atm. The buffer gas is continuously flowed into the sealed housing of the drift chamber via the “forward” and “contra” flows, as labeled in Fig. 1, and leaves the chamber via the “exhaust.” The contra flow contains any added attaching gas, whilst the forward flow is pure buffer gas. The glass envelope around the ring electrodes is used to constrain the

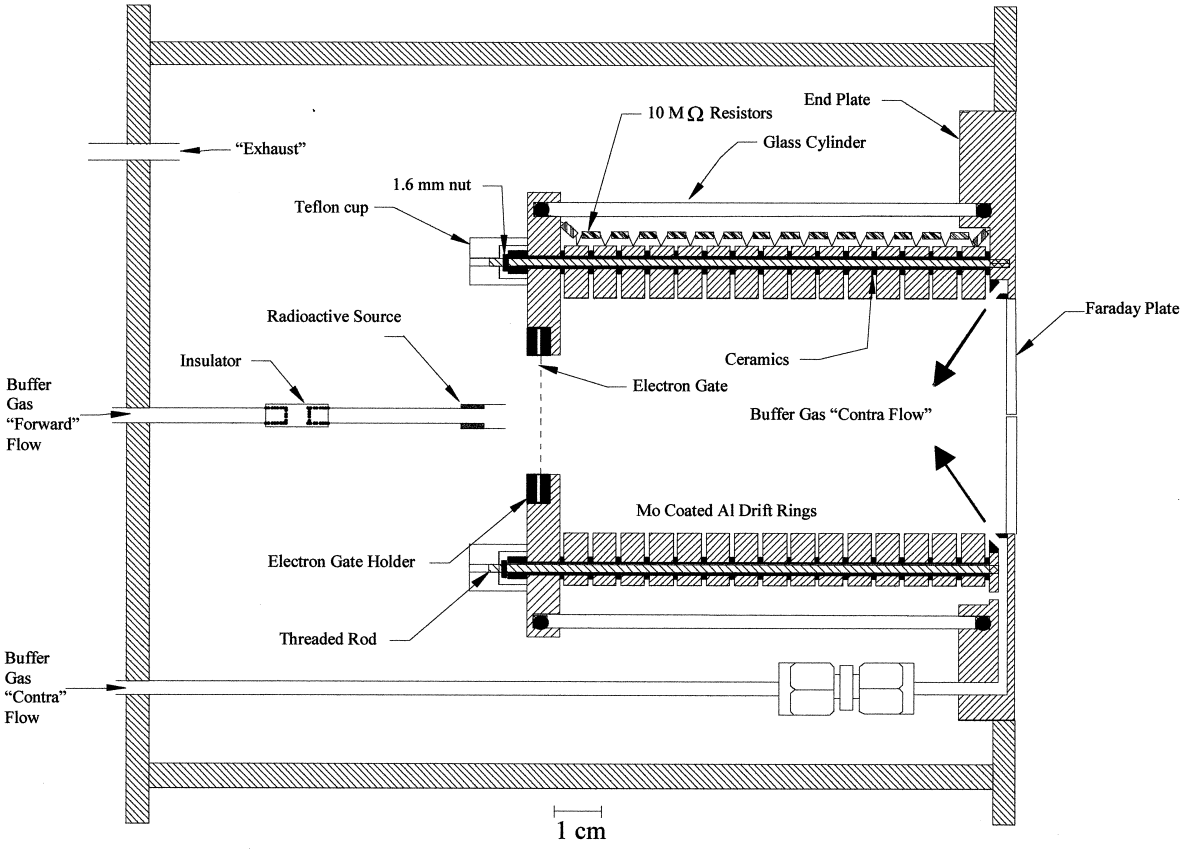

Fig. 1. A schematic diagram of the upgraded Birmingham electron-swarm drift tube. The diagram represents a cross section of the cylindrically symmetric drift tube.

contra flow in a direction toward the electron gate. The contra gas supply also flows into the region between the rings and glass tube via holes in the end plate. This means that no gas becomes trapped, and hence permits rapid change of the attaching gas concentration in the drift tube.

2.4. Electron source

We have made no modification to the electron source. In brief, electrons are constantly produced by ionisation of the nitrogen buffer gas by high-energy β particles emitted from a 11 mCi ^{63}Ni radioactive source which is placed at the end of an electrically isolated tube used to supply the forward flow of the buffer gas (see Fig. 1). As in the original instrument, a negative high voltage is applied to the source. For $E/N > 3 \times 10^{-18}$ V cm^2, the voltage difference between the source and the electron gate is such that the electric field strength is the same as inside the drift tube. However, for lower drift fields, a higher electric field strength is necessary to improve the migration of electrons to the gate, and hence into the main drift region.

The distance from the source to the electron gate is approximately one tenth of the total drift length. Given this, and the use of a forward flow to inhibit penetration of the attaching gas into the region between the source and the electron gate, it is reasonable to assume that little attachment occurs before electrons pass through the electron gate. Thus the flux of electrons reaching the electron gate will be indepen-

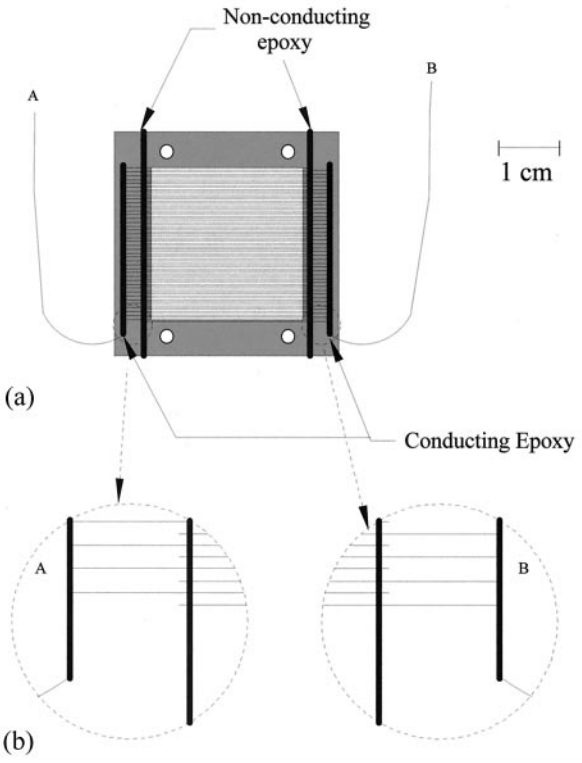

Fig. 2. (a) Design of the new interdigitated Bradbury-Nielsen electron gate. When the gate is closed there is a potential difference of 18 V between consecutive wires in the gate. One set of wires is 9 V above the drift tube entrance potential, the other set is 9 V below the drift tube entrance potential. To open the gate, both sets of wires are brought to the drift tube entrance potential. (b) A detailed view of the wires forming the arrays of the electron gate.

dent of the concentration of the attaching gas in the drift tube.

2.5. Electron gate

The second major modification to the original instrument is to the electron gate and its associated pulsing electronics, which together convert the constant stream of electrons produced in the source region into a chain of pulses. A schematic diagram of the new gate is presented in Fig. 2(a). It is based on the Bradbury–Nielsen design [31], consisting of two sets of interdigitated wire arrays, labeled A and B in Fig. 2. When a sufficient potential difference exists between the arrays, electrons passing through the gate will experience a large electric field deflecting them sideways and this will stop them from entering the drift tube.

To construct the gate, a 1.6 mm thick piece of epoxy glass circuit board with a square hole (25×25 mm^2) in the centre, was used as a base. Molybdenum wire (thickness 0.05 mm) was placed on top of this base with a spacing of 0.32 mm between consecutive wires (this spacing being imposed by the pitch of two M1.6 threaded rods placed on opposite ends of the circuit board). Whilst held taut, the wires were glued in place by nonconducting epoxy resin. The single set of wires was separated into two interdigitated sets by cutting every other wire between the nonconducting epoxy strip and the threaded rod, starting with the first wire on one end and the second wire on the other end. The wires from each set were then joined together using conducting epoxy resin [see Fig. 2(b)]. Any excess wire was removed to prevent the possibility of having short circuits. Thus, a fully interdigitated grid was produced with electrical connections on either side of the wire arrays. The resulting electron gate was mounted into the electron gate holder (see Fig. 1). As a result of the fine grid spacing achieved (0.32 mm), only a small potential difference ($<$18 V) between the wire sets A and B is needed to stop electrons entering the drift tube for electric field strengths up to about 450 V cm^{-1} (corresponding to an $E/N \approx 2 \times 10^{-17}$ V cm^2).

In comparison, our previous gate consisted of two parallel wire arrays isolated from each other by a thin polytetrafluoroethylene spacer. To close this gate, a potential difference of up to 100 V between the arrays was needed. Successful operation of this gate demanded careful matching of several parameters. These included the amplitude of the voltage pulse (to open the gate), the potential difference between the two arrays (to hold the gate closed) and the high voltages supplied to the source and to the drift tube voltage divider network. Easy operation of the instrument was only possible by the computer control of all the necessary voltages [32]. Furthermore, the operation of the electron gate proved to be extremely troublesome for $E/N < 2 \times 10^{-18}$ V cm^2.

A major advantage of our new electron gate is that

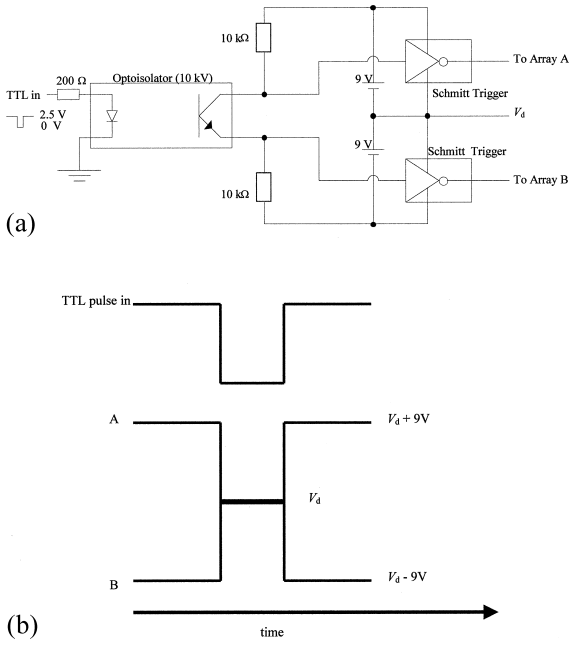

Fig. 3. (a) Circuit diagram of the pulsing electronics for the electron gate. (b) Schematic representation of the voltages on the wire arrays A and B as a TTL pulse is applied to the optoisolator.

no adjustment to the potential difference applied between the wire arrays is required over the entire range of electric field strengths used. This greatly simplifies the operation of the instrument. Further the performance of the gate is independent of E, and in particular well-shaped electron pulses are obtained with $E/N < 2 \times 10^{-18}$ V cm^2.

With the new design, to hold the electron gate closed, the potential on array A is held at 9 V above the drift tube entrance potential (V_d), while array B is held at a potential 9 V below V_d. To open the gate, the potentials on arrays A and B are simultaneously switched to V_d. Thus, the amplitude of each individual switching pulse is only 9 V. These pulses are easily produced by feeding a standard TTL pulse via a 10 kV optoisolator into a simple network of two Schmitt triggers. Details of the circuit used are shown in Fig. 3(a). Representations of the TTL pulse supplied to the optoisolator, and the voltage pulses supplied to wire sets A and B to open the gate, are illustrated in Fig. 3(b). The Schmitt triggers provide a very fast rise/fall time (ns) for the pulses to the electron gate. Schmitt trigger circuitry could not have been used to produce the large voltage pulses needed for our earlier electron gate. Thus, a second major advantage of the new gating system is that the pulses have much faster rise and fall times than was previously available. The switching time of the original electron gate was limited to about 20 μs because of the large pulse amplitude (~100 V) typically required to activate it.

The new pulsing electronics and electron gate system give the electron pulse a well-defined start time. Hence, electron drift velocities can be determined and compared with those obtained theoretically by Hunter et al. [10]. This is important because such comparisons permit a detailed characterisation and validation of our system. This is discussed further.

Electron pulse widths of 0.2–1 ms are usually used with a gap of about 40 ms between pulses, so that the instrument operates at a frequency of about 25 Hz. The arriving pulse is detected on the Faraday plate.

2.6. Detection amplifier

The Faraday plate collects the electrons and anions that have passed through the drift region. The current is converted to a voltage by a current to voltage converter. The resulting voltage is then amplified to give a total gain of about 10^9 V A^{-1}. The amplified signal is passed either to a transient digitiser (to monitor its temporal profile) or to a gated integrator (to measure its amplitude).

The amplification scheme imposes a time constant. This time constant was investigated by supplying to the amplifier a sharp current pulse [full width at half maximum (FWHM) < 1 μs] and monitoring the resulting output to produce an amplifier response function. This is illustrated in Fig. 4(a). A convolution of this response function with a recording of the voltage pulse applied to the electron gate, Fig. 4(b), is shown in Fig. 4(c). This exactly reproduces the experimentally observed profile of the voltage pulse from the detection amplifier due to the arrival of a pulse of electrons [illustrated in Fig. 4(d), measured at $E/N = 3.2 \times 10^{-19}$ V cm^2)]. Note that the convoluted curve [Fig. 4(c)] has been shifted along the time

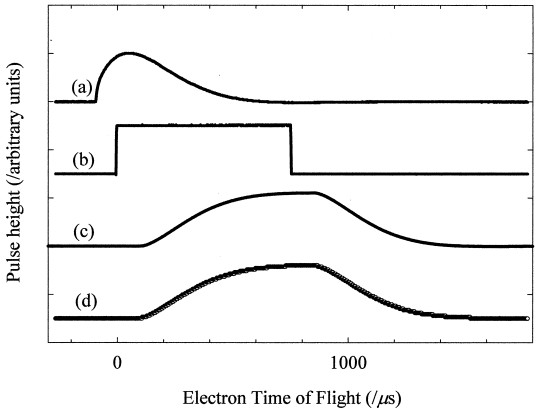

Fig. 4. (a) Recorded amplifier response to a current pulse of FWHM < 1 μs. (b) Recording of the voltage pulse applied to the electron gate. (c) A convolution of (a) and (b) illustrating the expected shape of the electron pulse after amplification and detection. This modified pulse has been shifted along the time axis to lie above (d). (d) The experimentally recorded electron pulse ($E/N = 3.2 \times 10^{-19}$ V cm^2) from the detection amplifier.

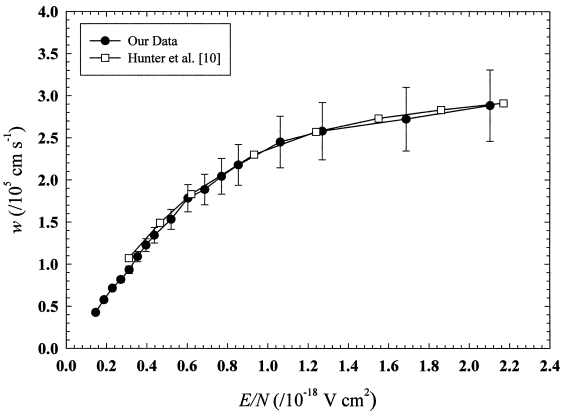

Fig. 5. Mean electron drift velocities, w, extracted from data such as that represented in Fig. 4, and compared against published values [10], as a function of E/N. The error bars shown reflect the uncertainties in the measurements of the electron pulse drift times.

axis so that it lies on top of the experimentally measured curve [Fig. 4(d)]. This shift represents the drift time of the pulse of electrons through the drift tube for this E/N. For these timing measurements, a suppressing grid was installed at a distance d ($\sim$3 mm) in front of the Faraday plate to minimise any image current. The grid was maintained at a potential of $d \times E$ to minimise any distortion of the E field in the drift tube.

2.7. Determination of mean electron drift velocities

As mentioned previously, the study of the temporal behaviour of the arriving electron pulses—a development made possible by the fast switching provided by our new interdigitated gate and pulsing electronics—allows the mean time-of-flight of the electrons through the drift tube to be determined. From these measurements, and knowing the drift length, the mean electron drift velocities, $w(E/N)$, for various E/N's can be calculated. The mean electron drift velocity is a measurable probe of the electron energy distribution. Thus, these measurements not only provide useful information, which is required for the determination of electron attachment rate constants from the measured density normalised electron attachment coefficients, but also provide a validation of our drift tube technique for investigating electron attachment processes. Fig. 5 is a plot of the experimentally derived mean electron drift velocities as a function of E/N ($<2 \times 10^{-18}$ V cm^2), compared to the values obtained by Hunter et al. [10] from an approximate numerical solution to the Boltzmann transport equation for electrons in nitrogen. The agreement is very good, and allows us to conclude that the E field is uniform in our drift tube, and any distortion in its uniformity has little or no effect on the electron energy distribution at each E/N. Furthermore, any impurities in the nitrogen buffer gas do not significantly alter the electron energy distributions. For higher E/N ($>2 \times 10^{-18}$ V cm^2), the mean electron drift velocities become increasingly difficult to measure by our technique, because of the shorter electron pulse drift times. Therefore at present, we only feel confident in using our electron time-of-flight data to obtain the mean electron drift velocities for $E/N \leq 2 \times 10^{-18}$ V cm^2. Values of mean electron drift velocities for higher E/N's are taken from the results of Hunter et al. [10]. Tables 1 and 2 contain the values of $w(E/N)$, used to determine the electron attachment rate constants from the measured density normalised electron attachment coefficients for SeF_6 and TeF_6, respectively.

Table 1
Density normalised electron attachment coefficients (α) and electron attachment rate constants (k_a) for SeF_6 in an atmospheric pressure nitrogen buffer gas as a function of E/N and mean electron energy ($\bar{\epsilon}$). The mean electron energies and mean electron drift velocities (w) for each E/N have been taken from data presented in an article by Hunter et al. [10]. The exceptions are the mean electron drift velocities for $E/N < 2 \times 10^{-18}$ V cm^2 which were determined experimentally in this study.

E/N ($/10^{-18}$ V cm^2)	$\bar{\epsilon}$ (/eV)	w ($/10^5$ cm s^{-1})	α ($/10^{-16}$ cm^2)	k_a ($/10^{-11}$ cm^3 s^{-1})
0.425	0.04	1.31	61.5	80.2
0.833	0.05	2.14	33.2	71.2
1.242	0.07	2.56	24.8	63.5
1.650	0.08	2.74	20.6	56.6
2.059	0.09	2.87	18.3	52.6
2.467	0.11	2.97	16.2	48.1
2.876	0.12	3.06	13.8	42.2
3.284	0.13	3.16	13.0	41.0
3.693	0.15	3.25	11.6	37.7
4.101	0.16	3.34	10.3	34.3
4.510	0.17	3.43	9.3	31.8
4.918	0.19	3.52	8.1	28.7
5.327	0.20	3.61	7.1	25.6
5.735	0.22	3.69	6.7	24.9
6.144	0.23	3.77	6.3	23.8
6.552	0.24	3.85	5.9	22.9
6.961	0.26	3.93	5.4	21.3
7.369	0.27	4.01	5.0	20.1
7.778	0.28	4.09	4.7	19.1
8.186	0.30	4.17	4.3	17.8
8.595	0.31	4.25	3.9	16.6
9.003	0.32	4.30	3.7	15.9
9.412	0.34	4.36	3.5	15.1
9.820	0.35	4.42	3.2	14.4
10.229	0.36	4.49	3.0	13.4
10.637	0.38	4.55	2.9	13.0
11.046	0.39	4.61	2.7	12.4
11.454	0.40	4.68	2.5	11.8
11.863	0.42	4.74	2.3	11.1
12.271	0.43	4.80	2.2	10.8
12.680	0.44	4.86	2.2	10.8
13.088	0.45	4.93	2.0	9.9
13.497	0.46	4.99	2.0	9.7
13.905	0.47	5.05	1.8	9.2
14.314	0.49	5.12	1.7	8.8
14.722	0.50	5.18	1.6	8.4
15.131	0.51	5.25	1.5	8.1
15.539	0.52	5.31	1.5	7.8
15.948	0.53	5.37	1.4	7.5
16.356	0.54	5.44	1.3	7.2

2.8. Mass spectrometric analysis of the anion products

No changes to the original apparatus, or to the data acquisition, have been made for the detection and recording of the anion products [5]. Therefore, only a brief summary will be given here.

To determine the anion products resulting from electron attachment, a constant stream of electrons is allowed to enter the drift tube by leaving the electron gate open. Anions, produced from the electron attachment process, drift under the influence of the electric field toward the Faraday plate. Upon arrival at the Faraday plate, a small fraction of the anions are

Table 2
Density normalised electron attachment coefficients (α) and electron attachment rate constants (k_a) for TeF_6 in an atmospheric pressure nitrogen buffer gas as a function of E/N and mean electron energy ($\bar{\epsilon}$). The mean electron energies and mean drift velocities (w) for each E/N value have been taken from data presented in an article by Hunter et al. [10]. The exceptions are the mean electron drift velocities for $E/N < 2 \times 10^{-18}$ V cm^2 which were determined experimentally in this study.

E/N ($/10^{-18}$ V cm^2)	$\bar{\epsilon}$ (/eV)	w ($/10^5$ cm s^{-1})	α ($/10^{-17}$ cm^2)	k_a ($/10^{-12}$ cm^3 s^{-1})
0.415	0.04	1.28	63.9	81.8
0.831	0.05	2.14	31.4	67.2
1.246	0.07	2.57	25.0	64.2
1.662	0.08	2.74	21.9	60.0
2.077	0.09	2.87	16.7	47.9
2.493	0.11	2.97	15.2	45.2
2.908	0.12	3.07	12.8	39.4
3.324	0.13	3.17	11.3	35.9
3.739	0.15	3.26	10.5	34.4
4.155	0.16	3.35	9.6	32.2
4.570	0.18	3.44	8.9	30.8
4.986	0.19	3.53	8.3	29.2
5.401	0.20	3.62	7.4	27.0
5.817	0.22	3.71	6.9	25.6
6.232	0.23	3.79	6.2	23.7
6.648	0.25	3.87	5.6	21.8
7.063	0.26	3.95	5.2	20.7
7.479	0.27	4.03	4.9	19.6
7.894	0.29	4.11	4.5	18.5
8.310	0.30	4.19	4.1	17.2
8.725	0.32	4.27	3.8	16.0
9.141	0.33	4.33	3.6	15.4
9.556	0.34	4.39	3.3	14.3
9.971	0.36	4.45	3.1	13.8
10.387	0.37	4.51	2.9	13.2
10.802	0.38	4.57	2.8	12.6
11.218	0.40	4.64	2.6	12.0
11.633	0.41	4.70	2.4	11.4
12.049	0.42	4.76	2.4	11.3
12.464	0.43	4.82	2.2	10.4
12.880	0.45	4.89	2.1	10.3
13.295	0.46	4.95	2.1	10.2
13.711	0.47	5.01	1.9	9.7
14.126	0.48	5.07	1.9	9.4
14.542	0.49	5.14	1.8	9.1
14.957	0.50	5.20	1.7	8.7
15.373	0.51	5.26	1.7	8.9
15.788	0.52	5.33	1.7	9.0
16.204	0.53	5.39	1.5	8.0
16.619	0.54	5.45	1.4	7.5

carried by the buffer gas through the 70 μm pinhole, located centrally in the plate, to the differentially pumped region. A fraction of these anions are then focused into the quadrupole mass spectrometer via a skimmer cone.

Branching ratios of the product anions from electron attachment are obtained by extrapolating product anion signals to zero neutral attaching gas number density. This takes into account any reactions of the product anions with the neutral attaching gas. Only two product anions were observed in the studies presented here. Branching ratios were measured with the detection quadrupole operating at its lowest resolution. This allowed easy separation of the product

anions [their masses differ by 19 u (corresponding to the mass of a fluorine atom)], and made mass discrimination negligible.

2.9. Sample preparation and injection

Stainless steel cylinders (volume $\sim 2 \times 10^3$ cm^3), which have been silcosteel treated (Restek Corporation) to passivate the surfaces, are used to store the attaching gas in concentrations of typically a few hundred parts per million in nitrogen gas (zero grade, 99.998%) at a total pressure of about 2 atm. Gases in the cylinders are continuously mixed by a small circulation pump to ensure homogeneity. During an experiment, a gas sample of known concentration is transferred from the storage cylinder, and injected into the contra flow, which typically flows at 400 cm^3 min^{-1} at slightly above atmospheric pressure. The sample injection is controlled by using a digital infusion syringe pump. The "forward" flow of pure nitrogen gas is typically flowing at 100–150 cm^3 min^{-1}, also at slightly above atmospheric pressure. The pressure and gas temperature in the drift chamber are measured so that the number densities of nitrogen and the electron attaching gas in the drift tube can be calculated from the ideal gas equation.

2.10. Measuring α at a single E/N

The determination of α for a single E/N requires the measurement of electron pulse amplitudes A as a function of attaching gas concentration $[M]$. α is obtained by fitting these amplitudes to the simple linear relationship:

$$\ln A = \ln A_0 - \alpha l[M] \quad (7)$$

The use of a constant pressure of N_2 buffer gas, and a ^{63}Ni source of β particles ensures that A and A_0 are constant for a given E/N and $[M]$.

Electron current pulses, with widths of typically 0.7 ms, are produced at a frequency of 25 Hz. The amplitude (A) of the amplified signal from the detection amplifier, produced by each electron current pulse is measured using a gated integrator. The width of the gate is much shorter (3 μs) than the detected pulse, and the gate is positioned temporally to coincide with the centre of the arriving detected voltage pulse. Amplifier baseline offset correction is achieved by recording the detected voltage signal with the integrator's gate moved to 1–2 ms after the end of the detected electron pulse. The gated integrator provides the first stage of averaging. For each pulse, the output voltage from the integrator is passed to a computer. The average of 100 measurements is formed, and the baseline correction applied to give A for a given $[M]$.

The concentration of the attaching gas is then changed by altering the rate at which the dilute mixture of the attaching gas is injected into the contra flow of N_2. The new concentration of attaching gas in the drift tube is established after about 5 min (as deduced by observing the response of the voltage amplitude of the pulses from the detection amplifier) and measurements of the detected electron pulse amplitudes are typically made 10 min after changing the injection rate.

For each E/N, measurements are made at 5–8 concentrations (including $[M] = 0$). The maximum concentration is chosen to produce an attenuation of the pulse amplitude of about 70%. Initially the appropriate concentrations have to be determined empirically. A linear least-squares fit of the data to Eq. (7), with all points weighted equally, gives $\alpha(E/N)$.

2.11. Recording a data set: α as a function of E/N

One approach to building a data set for $\alpha(E/N)$ would be to repeat the cycle of measurements described above at a sequence of values for E/N. However, because of the long times required to change attaching gas concentrations compared to the short times needed to establish a new electric field E (made possible by the modifications to the drift tube and electron gate), this is an inefficient approach. Instead for each concentration of the attaching gas, the detected voltage pulse amplitude is measured as a function of E/N at intervals over a specified range. All

the high voltages, which need adjusting when changing the electric field strength in the drift tube, are computer controlled. This provides both precision and speed in the measurements. The data are then stored, the concentration of the attaching gas is changed, and the detected electron pulse voltage amplitudes measured for the same set of values of E/N. At the end of the experiment the voltage pulse amplitudes as a function of attaching gas concentration for each E/N are extracted from the accumulated data, and used to determine $\alpha(E/N)$.

2.12. Gas samples

Samples of the three compounds investigated in this study were commercially purchased (Fluorochem Limited, Derbyshire, UK) with the following stated purities: sulphur hexafluoride (99+%), selenium hexafluoride (99%) and tellurium hexafluoride (99+%). They were used directly without additional purification.

3. Results and discussion

For the buffer gas N_2, which was used exclusively in this study, the E/N range accessible with the present configuration of the instrument is $(0.4–18) \times 10^{-18}$ V cm^2. This corresponds to mean electron energies from 0.04 to 0.6 eV [10].

3.1. Density normalised electron attachment coefficients and electron attachment rate constants

For SF_6, SeF_6, and TeF_6, each set of raw data gave a good fit to Eq. (7). This is in accord with the general attachment mechanism outlined in the introduction [Eqs. (1)–(4)]. It also implies that, although the cross section for the removal of electrons by attachment is dependent on their energies, the combined effects of the accelerating field and collisions of the electrons with the nitrogen buffer gas are able to maintain a constant electron energy distribution.

Tables 1 and 2 present the results of the measurements for SeF_6 and TeF_6, respectively. Extensive tables of $\alpha(E/N)$ and $k_a(E/N)$ for SF_6 in N_2 have already been published [10], and our results are in good agreement with these. The density normalised electron attachment coefficients, $\alpha(E/N)$, as a function of E/N, for SF_6, SeF_6, and TeF_6 are plotted in Figs. 6(a)–6(c), respectively. Mean electron energies, used to provide the upper scales, were obtained from the tables of Hunter et al. [10].

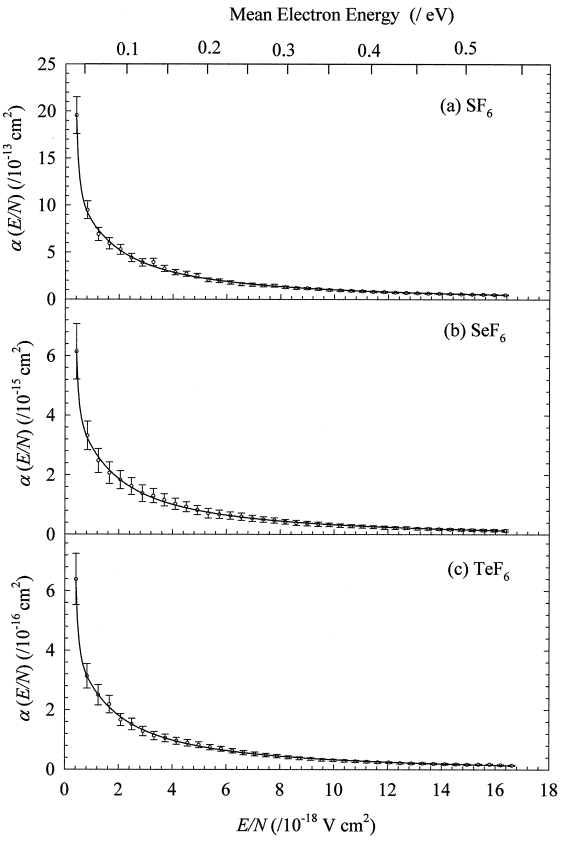

Fig. 6. The experimental density normalised electron attachment coefficients, α, as a function of E/N in an atmospheric pressure nitrogen buffer gas for the molecules (a) SF_6, (b) SeF_6, and (c) TeF_6. The points represent an average of six independent measurements, and the error bars shown represent one standard deviation about the mean value.

By multiplying the density normalised electron attachment coefficients by the appropriate mean electron drift velocities, the electron attachment rate constants, $k_a(E/N)$, are obtained. Plots of $k_a(E/N)$, as a function of E/N, for SF_6, SeF_6, and TeF_6 are presented in Figs. 7(a)–7(c), respectively.

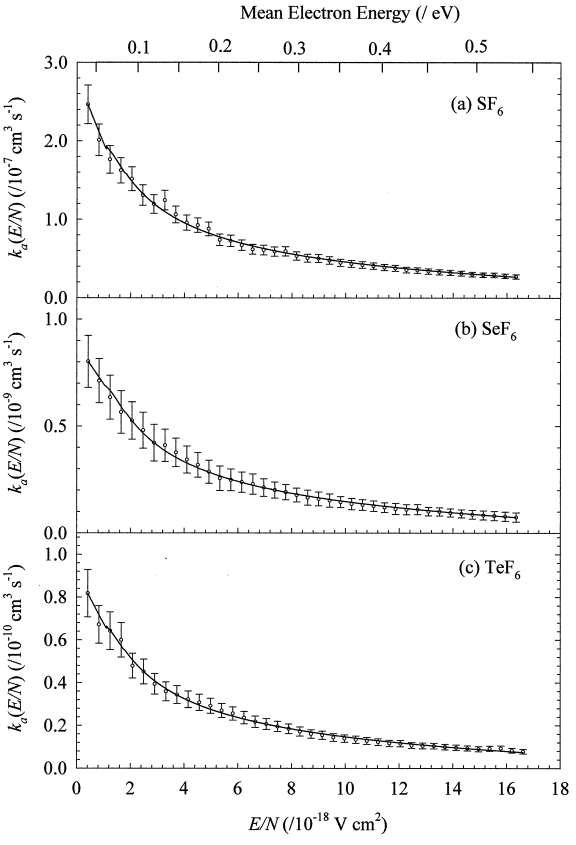

Fig. 7. The electron attachment rate constants, k_a, as a function of E/N in an atmospheric pressure nitrogen buffer gas for the molecules (a) SF_6, (b) SeF_6, and (c) TeF_6. The points represent an average of six independent measurements, and the error bars shown represent one standard deviation about the mean value.

From Figs. 6 and 7 it can be seen that the $\alpha(E/N)$ and $k_a(E/N)$ curves, respectively, for the three molecules possess similar shapes, i.e. the ratios of rate constants are to within experimental error independent of E/N. Given this similarity in the curves, we must demonstrate that there is no SF_6 trace impurity in our samples of SeF_6 and TeF_6. For example, if SeF_6 and TeF_6 have extremely low attachment rate constants ($<10^{-12}$ cm^3 s^{-1}), an impurity of SF_6 at the level of about 0.3% and 0.03% in the SeF_6 and TeF_6 samples, respectively, would result in the observed measurements. Reactions of SF_6^- with SeF_6 or TeF_6 would likely lead to the observed anion products discussed below. Mass spectrometric analyses made on the samples using a VG Pro Spec Mass Spectrometer, ruled out this problem because no SF_6 was detected in either of the samples. Indeed, the analysis revealed no identifiable impurities with masses $\geq$40 u (the starting mass on the spectrometer), and relative concentrations $\geq$0.1%.

The dependence of k_a on E/N for all three molecules indicates that the electron attachment cross sections are strongly peaked at $\epsilon = 0$. This is well established for SF_6 [10] and is supported by low-pressure electron beam studies for SeF_6 and TeF_6 [24,25]. The large differences in the values of $k_a(E/N)$ between SF_6, SeF_6, and TeF_6, suggest either that the electron autodetachment rate for the initially formed $(SeF_6^-)^*$ and $(TeF_6^-)^*$ is much higher than it is for $(SF_6^-)^*$, or (and more likely) maybe a result of poor vibrational overlap of the neutral and anion. The results for the three molecules suggest an inverse correlation between k_a and electron affinity, for the electron affinities of SeF_6, 2.9 $\pm$ 0.2 eV [26], and TeF_6, 3.3 $\pm$ 0.2 eV [27], are larger than that of SF_6, 1.05 $\pm$ 0.05 eV [8,33].

Our lowest E/N (4.0×10^{-19} V cm^2) will give to a good approximation a Maxwellian distribution of electron energies, with a mean electron energy of 0.042 eV. This mean electron energy is close to $\bar{\epsilon}$ for thermalised electrons at 300 K, 0.038 eV. It is then reasonable to suggest that $k_{th}(300\ K) \approx k_a(300\ K, E/N = 4.0 \times 10^{-19}$ V cm^2). Adopting this procedure, $k_{th}(SF_6) \approx (2.5 \pm 0.3) \times 10^{-7}$ cm^3 s^{-1}, $k_{th}(SeF_6) \approx (8.0 \pm 1.2) \times 10^{-10}$ cm^3 s^{-1}, and $k_{th}(TeF_6) \approx (8.2 \pm 1.1) \times 10^{-11}$ cm^3 s^{-1}. Our estimated SF_6 thermal electron attachment rate constant is in good agreement with the value of $(3.1 \pm 0.5) \times 10^{-7}$ cm^3 s^{-1}, obtained by Smith et al. [6] using a flowing afterglow technique, and $(2.3 \pm 0.1) \times 10^{-7}$ cm^3 s^{-1}, obtained by Hunter et al. [10] using an electron-swarm technique in a nitrogen buffer gas. The value we obtained for SeF_6 agrees less favourably with that obtained from an electron-swarm experiment operated under zero electric field conditions, $k_{th}(SeF_6) = 1.27 \times 10^{-9}$ cm^3 s^{-1} [28]. However, a direct comparison with this measurement may not be meaningful. The zero electric field experiment, in which the electrons are assumed to have a Maxwellian (thermal) energy distribution, was performed in pure

SeF_6 at a pressure of 8 Torr. Our experiment, on the other hand, consisted of a nitrogen buffer gas at atmospheric pressure seeded with a small quantity of SeF_6. Collisional stabilisation is an important process in electron attachment, competing with autodetachment, and can account for differences in k_a from experiments performed under different pressure and buffer gas conditions. An interpretation of the higher $k_{th}(SeF_6)$ obtained from the low-pressure, pure SeF_6 experiment is that SeF_6 stabilizes $(SeF_6^-)^*$ much more rapidly than N_2. A difference in the thermal electron attachment rate constants is also observed for electron attachment to TeF_6. Only an upper limit to the thermal electron attachment rate constant was determined by Davis et al. [28], $k_{th}(TeF_6) < 2 \times 10^{-11}$ cm^3 s^{-1}, which is much lower than the value we have measured in the high-pressure environment of our drift tube. This is presumably because of the reduced collisional stabilisation of $(TeF_6^-)^*$ in the earlier swarm measurements, which used 0.5 Torr of pure TeF_6.

3.2. Anion products resulting from electron attachment

Typical mass spectra recorded for SF_6, SeF_6, and TeF_6 can be seen in Figs. 8(a)–8(c), respectively. These were recorded at less than 1 u resolution so that the peaks associated with all the isotopes are well defined. For these mass spectra an $E/N = 8.2 \times 10^{-18}$ V cm^2, and $[SF_6] = 1.2 \times 10^{11}$ cm^{-3}, $[SeF_6] = 1.9 \times 10^{14}$ cm^{-3}, and $[TeF_6] = 7.6 \times 10^{13}$ cm^{-3} were used. Only two anion products resulting from electron attachment to the attaching molecules were observed. Nondissociative electron attachment leads to the formation of the parent anion, following collisional stabilisation by the nitrogen buffer gas:

$$e^- + XF_6 \rightarrow (XF_6^-)^* \xrightarrow{N_2} XF_6^- \quad (8)$$

while dissociative electron attachment leads to XF_5^-:

$$e^- + XF_6 \rightarrow (XF_6^-)^* \rightarrow XF_5^- + F \quad (9)$$

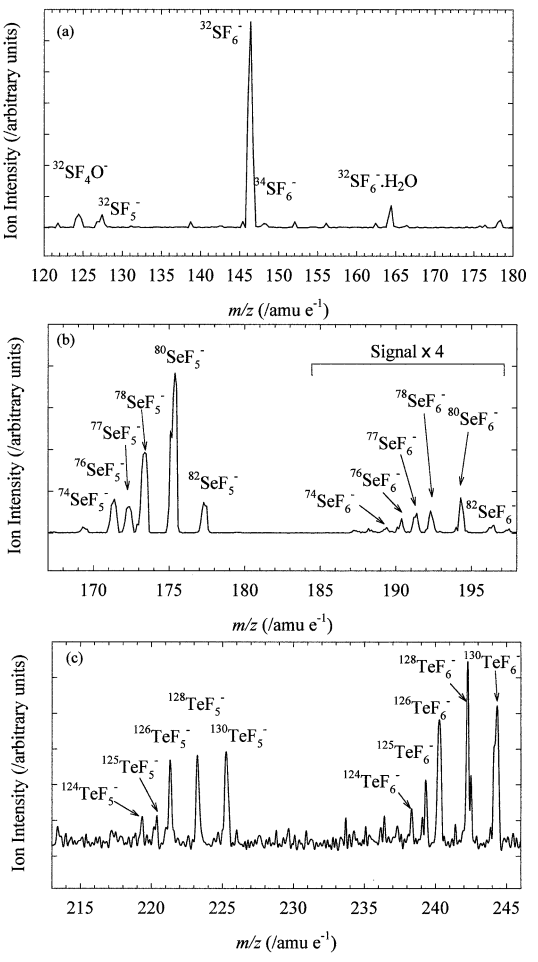

Fig. 8. High resolution recordings of the mass spectra resulting from electron attachment to (a) SF_6, (b) SeF_6, and (c) TeF_6 in an atmospheric pressure nitrogen buffer gas. The various sulphur, selenium, and tellurium isotopes are highlighted. Similar spectra were obtained for all E/N values. For SeF_6 and TeF_6 the relative intensities of the two anion products are very sensitive to the anion molecule reaction: $XF_6^- + XF_6 \rightarrow XF_5^- + (XF_6 + F)$. Thus (b) and (c) do not represent the product anion branching ratios in the swarm environment. These can only be determined by extrapolating the anion intensities to zero attaching gas concentration. For the spectra presented here $E/N = 8.2 \times 10^{-18}$ V cm^2 and $[SF_6] = 1.2 \times 10^{11}$ cm^{-3}, $[SeF_6] = 1.9 \times 10^{14}$ cm^{-3}, and $[TeF_6] = 7.6 \times 10^{13}$ cm^{-3}. A wider mass scale is shown for the SF_6 mass spectrum to illustrate the level of the "impurity" anions resulting from the reaction of SF_6^- with impurities in our nitrogen buffer gas and/or in our gas sample.

where X = S, Se, or Te. XF_5^- could also be produced through reaction 3(a). No other anion products resulting directly from electron attachment were observed.

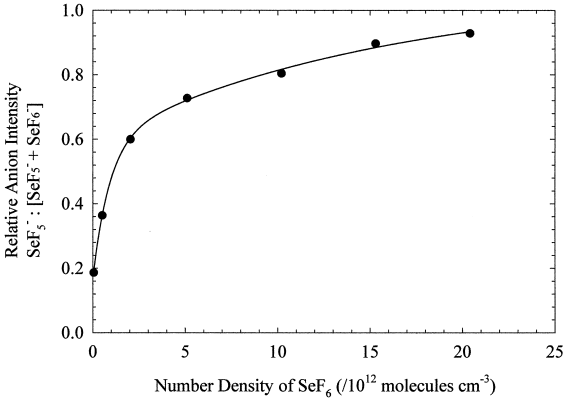

Fig. 9. An example of the effects of attaching gas concentration on the anion intensities is illustrated for SeF_6 at an E/N of 1.7×10^{-18} V cm^2. SeF_6 is chosen for this illustration, because it shows the greatest change in the relative anion intensity with changes in concentration. At extremely low concentrations of SeF_6 ($[SeF_6] < 1.5 \times 10^{12}$ cm^{-3}), SeF_6^- becomes the dominant anion product. The first point on the curve corresponds to $[SeF_6] = 5 \times 10^{10}$ cm^{-3}. Extrapolation back to $[SeF_6] = 0$ yields a SeF_5^- branching ratio of (16 ± 5)%.

Anion–molecule reactions can, and do, play a significant role in the high-pressure swarm environment, modifying the product anion branching ratios. Care therefore must be taken when determining the product anion branching ratios. In this investigation, for SeF_6 and TeF_6, the following anion–molecule reaction was observed:

$$XF_6^- + XF_6 \xrightarrow{k_{10}} XF_5^- + (XF_6 + F) \qquad (10)$$

the neutral product(s) being uncertain. An example of the effects of the reaction of XF_6^- with XF_6 on the anion intensities is illustrated in Fig. 9 for SeF_6 at an $E/N = 1.7 \times 10^{-18}$ V cm^2. SeF_6 is the most affected by reaction (10), and only at extremely low concentrations does SeF_6^- become the dominant anion. Thus, to obtain anion product branching ratios for electron attachment to SeF_6 and TeF_6, it was necessary to record the anion intensities as a function of attaching gas concentration and to extrapolate the results back to zero concentration. When the branching ratios are properly treated in this way, they are found to be relatively insensitive to E/N, at least over the range covered in this study, and our best estimates of the mean values are: SeF_6–SeF_5^- (20%), SeF_6^- (80%); and TeF_6–TeF_5^- (3%), TeF_6^- (97%).

For SF_6, reaction (10) was not observed for the concentrations of SF_6 used in this study. The reaction of SF_6^- with SF_6 to form SF_5^- + (SF_6 + F) is reported to be slow ($k_{10} < 10^{-12}$ cm^3 s^{-1}) [34]. To see any appreciable reaction, $[SF_6] > 1/k_{10}\tau \approx 3 \times 10^{13}$ cm^{-3}, where τ is the residence time of SF_6^- in the drift tube. This concentration is far greater than those used. Although reaction (10) caused no problems in determining the SF_5^- branching ratio, reactions of SF_6^- with impurities, either in the nitrogen buffer gas or in the sample added by injection, made estimation of the total yield of SF_6^- difficult. Consequently, in addition to SF_5^- and SF_6^-, the mass spectrum resulting from electron attachment to SF_6 contains several impurity anions, the majority of which are illustrated in Fig. 8(a). Due to the low electron affinity of SF_6, SF_6^- reacts with many molecules (A) by electron transfer:

$$SF_6^- + A \rightarrow A^- + SF_6 \qquad (11)$$

In contrast SF_5^- has been reported to react with relatively few molecules [35]. It was therefore assumed that all the anions resulting from the impurities were formed from reactions with SF_6^- so that the branching ratio for the production of SF_5^-:

$$\phi(SF_5^-) = \frac{I(SF_5^-)}{I(SF_5^-) + I(SF_6^-)} \qquad (12)$$

is calculated from the observed anion yields as

$$\phi(SF_5^-) = \frac{I_{obs}(SF_5^-)}{I_{obs}(SF_5^-) + I_{obs}(SF_6^-) + \Sigma\, I_{obs}(A^-)} \qquad (13)$$

For low E/N, the contribution of $\Sigma\, I_{obs}(A^-)$ to the SF_6^- anion intensity was typically about 20%, with this percentage reducing to about 10% for higher E/N. Fig. 10 shows the results of our experiments for three concentrations of SF_6. The observed proportion of SF_5^- is seen to be independent of the concentration of SF_6, confirming that reaction (10) does not affect the observations. The observed proportion of SF_5^- is observed to decrease as E/N increases. These results are in accord with an investigation conducted using our original instrument [5].

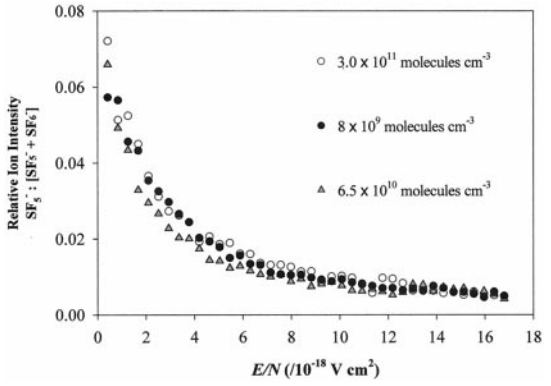

Fig. 10. Relative anion yield intensity for SF_5^- resulting from electron attachment to SF_6 in an atmospheric pressure nitrogen buffer gas for a range of E/N, at three different concentrations of SF_6. The rise in the observed proportion of SF_5^- with decreasing E/N is tentatively attributed to reactions of SF_6^- with unknown impurities in our system (see the text).

The existing results for electron attachment to SF_6 from low-pressure, electron beam experiments [13,14] can be used to predict how the SF_5^- branching ratio might vary with E/N in a swarm experiment. At the lowest electron energies the dominant product ion from electron attachment to SF_6 is SF_6^-; for electron energies above about 0.3 eV, the exclusive product is SF_5^-. In a swarm experiment, increasing E/N increases both the mean electron energy and the breadth of the electron energy distribution. The resulting qualitative prediction is that in a swarm experiment, the branching ratio for the production of SF_5^- will increase with increasing E/N. This expectation is in agreement with quantitative predictions obtained by convoluting the cross sections for the production of SF_5^- and SF_6^- (obtained from low-pressure, electron beam experiments [13]) with the E/N dependent electron energy distributions for a high-pressure swarm environment [10]. Both the qualitative and quantitative predictions neglect the possible effects of collisions of $(SF_6^-)^*$ with the nitrogen buffer gas. More sophisticated models of electron attachment, incorporating the effects of collisions have recently been proposed [36,37]. Although the application of these models is likely to influence the quantitative predictions [10], the assertion that the branching ratio for the production of SF_5^- will increase with increasing E/N is expected to remain valid. Our results disagree with the well-founded prediction presented above. Compared to the prediction, there appears to be an over production of SF_5^-, with the amount of "extra" SF_5^- increasing as E/N decreases. A contaminant anion at a $m/z = 127$ can be ruled out. The region around $m/z = 127$ was examined under high resolution and sensitivity, and shown to comprise of two peaks, one at $m/z = 127$ u (≈95%) and the other at $m/z = 129$ u (≈5%) due to $^{32}SF_5^-$ and $^{34}SF_5^-$, respectively. Their relative intensities show that the $m/z = 127$ u peak is SF_5^- and there is no significant contribution to this peak from impurity anions. A possible explanation of this observation is that SF_6^- is reacting by fluorine atom transfer with some impurity (B) in the buffer gas:

$$SF_6^- + B \rightarrow SF_5^- + BF \quad (14)$$

Fluorine atom transfer has been reported to occur in some reactions of SF_6^- [38]. As E/N decreases, the mean drift velocities of the anions will decrease. Thus, the residence times of the anions in the drift tube will increase, and the effects of any anion–molecule reactions such as reaction (14) will increase. We plan to conduct experiments with a higher purity sample of N_2 buffer gas to test this possible explanation of the observations.

SeF_6 and TeF_6 have quite high electron affinities, much higher than SF_6. Thus there are relatively few molecules with which SeF_6^- and TeF_6^- may react by electron transfer. The mass spectra showed very low yields of anions other than XF_5^- and XF_6^-. There have been no reports of reactions involving fluorine atom transfer from SeF_6^- or TeF_6^-. The E/N independent branching ratios for production of SeF_5^- (20%) and TeF_5^- (3%) resulting from electron attachment to SeF_6 and TeF_6, respectively, are thus believed to be the true branching ratios appropriate for the high-pressure swarm environment.

None of the low-pressure, electron beam studies [23–26] observed SeF_6^- or TeF_6^-, presumably because $(SeF_6^-)^*$ and $(TeF_6^-)^*$ are not long-lived enough to be detected before autodetachment or dissociation occurs. Brion [24] mentions that when a beam of low

energy electrons is passed through a sample of SeF_6 (TeF_6) to which some SF_6 has been added, then SeF_6^- (TeF_6^-) is formed. The suggested explanation was that the efficiency of collisional stabilisation of excited SeF_6^- (TeF_6^-) by SF_6 is very high. However, given the high concentration of SF_6 used in Brion's experiments, it is probable that anion–molecule reactions led to the formation of the parent anion, e.g. for SeF_6:

$$SF_6^- + SeF_6 \rightarrow SeF_6^- + SF_6 \quad (15)$$

rather than especially efficient collisional stabilisation of the excited parent anion by SF_6, e.g. for SeF_6:

$$e^- + SeF_6 \rightarrow (SeF_6^-)^* \xrightarrow{SF_6} SeF_6^- \quad (16)$$

We tried to confirm the above anion–molecule reaction (15) using our selected ion flow tube (SIFT) apparatus [39], but found it impossible to generate a pure swarm of SF_6^-. However, a SIFT study of the reactions of several other anions with SeF_6 and TeF_6 [40] is in agreement with the assignment. For example, O_2^- reacts with SeF_6 to give SeF_6^- (50%) and SeF_5^- (50%), and with TeF_6 to give TeF_6^- (100%). O^- reacts with SeF_6 to give SeF_6^- (92%) and SeF_5^- (8%), and with TeF_6 to give TeF_6^- (100%). The electron affinity of SF_6 (EA = 1.05 eV) is less than that of O (EA = 1.46 eV) but greater than that of O_2 (EA = 0.45 eV). Therefore we can reasonably expect SF_6^- to react with SeF_6 to produce predominantly SeF_6^- and with TeF_6 to produce only TeF_6^-.

Electron beam studies observed SeF_5^- and TeF_5^- to be the dominant [24] or only [25] anion product for low energy electron attachment to SeF_6 and TeF_6. As mentioned previously, these anion products are also observed by us, but are far from being the dominant species. Brion [24] also observed a weak Se^- signal due to zero energy electron attachment to SeF_6, which we did not observe.

4. Conclusions

Details of a modified electron-swarm mass spectrometric apparatus used for the study of electron attachment to molecules under swarm conditions have been presented. There are a number of benefits resulting from the modifications to the apparatus. These include the following: a reduction in the time required to acquire data, which allows us to screen the electron attachment properties of a wide range of molecules; no charging effects have been observed, providing us with more confidence in our electric field strengths; low E/N ($<10^{-18}$ V cm^2) can be easily reached, corresponding to mean electron energies approaching the thermal value; and the ability to look at the temporal behaviour of the electron pulses for $E/N \leq 2 \times 10^{-18}$ V cm^2, which has allowed us to validate our system, by determining mean electron drift velocities and comparing them against values in the literature [10].

Further validation of our system has been obtained by the SF_6 study presented here. The measured density normalised electron attachment coefficients and rate constants agree well with those obtained by Hunter et al., who used a different swarm apparatus [10].

The first detailed electron-swarm measurements of SeF_6 and TeF_6 have been presented in this article. Interesting differences in the electron attachment process between these molecules and SF_6 have been noticed. Whilst the anion products of electron attachment are the same [XF_6^- (dominant) and XF_5^-], with only slight variations in the product anion branching ratios as X is changed, the electron attachment rate constants for SeF_6 and TeF_6 are approximately 300 and 3000 times smaller, respectively, than those of SF_6 for all the E/N's covered in these experiments. The attachment rate data imply that electron attachment to the three molecules is dominated by a sharp zero-energy resonance in their electron attachment cross sections.

Acknowledgements

The authors are grateful to the Technological Plasma Initiative Program, EPSRC (grant no. GR/L82083) for the financial support of this work. They wish to thank Dr. P. Cameron (CBD, Porton Down, Salisbury) for his advice with regard to the design of the new drift tube. Finally, they are very grateful to P.

Ashton, Mass Spectrometry Facility, School of Chemistry, University of Birmingham for analysing the samples used in this study.

REFERENCES

[1] P. Chabert, T.E. Sheridan, R.W. Boswell, J. Perrin, Plasma Sources Sci. Technol. 8 (1999) 561.
[2] Database Needs for Modelling and Simulation of Plasma Processing Board on Physics and Astronomy, Commission on Physical Sciences, Mathematics, and Applications, National Research Council, National Academy Press, Washington, DC, 1996.
[3] L.G. Christophorou, Atomic and Molecular Radiation Physics, Wiley-Interscience, New York, 1971.
[4] A. Chutjian, A. Garscadden, J.M. Wadehra, Phys. Rep. 264 (1996) 393.
[5] Y. Liu, C.A. Mayhew, R. Peverall, Int. J. Mass Spectrom. Ion Processes 152 (1996) 225.
[6] D. Smith, N.G. Adams, E. Alge, J. Phys. B 17 (1984) 461.
[7] L.G. Christophorou, D.L. McCorkle, A.A. Christodoulides, in Electron-Molecule Interactions and their Applications, Vol. 1, Academic, New York, 1984, Chap. 6, pp. 496–617.
[8] E.P. Grimsrud, S. Chowdbury, P. Kebarle, J. Chem. Phys. 83 (1985) 1059.
[9] E.C.M. Chen, L.R. Shuie, E.D. D'sa, C.F. Batten, W.E. Wentworth, J. Chem. Phys. 88 (1988) 4711.
[10] S.R. Hunter, J.G. Carter, L.G. Christophorou, J. Chem. Phys. 90 (1989) 4879.
[11] T.M. Miller, A.E. Stevens-Miller, J.F. Paulson, X. Liu, J. Chem. Phys. 100 (1994) 8841.
[12] D. Klar, M.W. Ruf, H. Hotop, Chem. Phys. Lett. 189 (1992) 448.
[13] L.E. Kline, D.K. Davies, C.L. Chen, P.J. Chantry, J. Appl. Phys. 50 (1979) 6789.
[14] M. Fenzlaff, R. Gerhard, E. Illenberger, J. Chem. Phys. 88 (1988) 149.
[15] N. Mutsukura, G. Turban, Plasma Chem. Plasma Processes 10 (1990) 27.
[16] K.R. Ryan, E.C. Plumb, Plasma Chem. Plasma Processes 10 (1990) 207.
[17] I. Sauers, IEEE Trans. Electr. Insul. EI-21 (1986) 105.
[18] I. Sauers, Plasma Chem. Plasma Processes 8 (1988) 247.
[19] I. Sauers, H.W. Ellis, L.G. Christophorou, IEEE Trans. Electr. Insul. EI-21 (1986) 111.
[20] I. Sauers, L.G. Christophorou, S.M. Spyrou, Plasma Chem. Plasma Processes 13 (1993) 17.
[21] H.X. Wan, J.H. Moore, J.K. Olthoff, R.J. Van Brunt, Plasma Chem. Plasma Processes 13 (1993) 1.
[22] T.L. Williams, L.M. Babcock, N.G. Adams, Int. J. Mass Spectrom. 185 (1999) 759.
[23] W.M. Hickam, D. Berg, J. Chem. Phys. 29 (1958) 157.
[24] C.E. Brion, Int. J. Mass Spectrom. Ion Phys. 3 (1969) 197.
[25] J.A.D. Stockdale, R.N. Compton, H.C. Schweinler, J. Chem. Phys. 53 (1970) 1502.
[26] R.N. Compton, P.W. Reinhardt, C.D. Cooper, J. Chem. Phys. 68 (1978) 2023.
[27] R.N. Compton, C.D. Cooper, J. Chem. Phys. 59 (1973) 4140.
[28] A.F.J. Davis, R.N. Compton, D.R. Nelson, J. Chem. Phys. 59 (1973) 2324.
[29] J.E. Pollard, D.J. Trevor, Y.T. Lee, D.A. Shirley, Rev. Sci. Instrum. 52 (1981) 1837.
[30] D.A. Dahl, J.E. Delmore, SIMION PC Programme, Idaho National Laboratory, ID, 1991.
[31] L.G. Huxley, R.W. Crompton, The Diffusion and Drift of Electrons in Gases Wiley Series in Plasma Physics, Wiley-Interscience, New York, 1974, Chap. 10, pp. 297–370.
[32] G.J. Jarvis, Ph.D. thesis, University of Birmingham, 1998.
[33] E.C.M. Chen, J.R. Wiley, C.F. Batten, W.E. Wentworth, J. Phys. Chem. 98 (1994) 88.
[34] C. Lifshitz, T.O. Tiernan, B.M. Hughes, J. Chem. Phys. 59 (1973) 3182.
[35] Y. Ikezoe, S. Matsuoka, M. Takebe, A. Viggiano, Gas Phase Ion–Molecule Reaction Rate Coefficients Through 1986, Ion Reaction Research Group, The Mass Spectroscopy Society of Japan, (1987).
[36] D. Smith, P. Španel, S. Matejcik, A. Stamatovic, T.D. Märk, T. Jaffke, E. Illenberger, Chem. Phys. Lett. 240 (1995) 481.
[37] P. Španel, S. Matejcik, D. Smith, J. Phys. B: At. Mol. Opt. Phys. 28 (1995) 2941.
[38] G.E. Streit, J. Chem. Phys. 77 (1982) 826.
[39] D. Smith, N.G. Adams, Adv. At. Mol. Phys. 24 (1988) 1.
[40] R.A. Kennedy, C.A. Mayhew, unpublished.